Phase diagram in exchange-coupled CoTb/[Co/Pt] multilayer-based magnetic tunnel junctions

Mathias Bersweiler, Daniel Lacour, Karine Dumesnil, François Montaigne, Michel Hehn

Phase diagram in exchange-coupled CoTb/[Co/Pt] multilayer-based magnetic tunnel junctions

M. Bersweiler, D. Lacour, K. Dumesnil, F. Montaigne, and M. Hehn*
Institut Jean Lamour (UMR CNRS 7198), Université de Lorraine, Vandoeuvre-lès-Nancy, France
(Received 1 October 2015; published 28 December 2015)

Magnetic and magneto-transport properties of [Co/Pt]/MgO/[Co/Pt]CoTb magnetic tunnel junctions have been investigated. Depending on the thickness of the Pt layer, temperature, and field history, the [Co/Pt]CoTb hard layer shows complex behaviors that can be reproduced by micromagnetic calculations. The magnetic tunnel junctions appear to exhibit conventional behavior but also exchange bias and spring magnet and domain duplication phenomena that have been observed combining magnetometry and interface-sensitive spin-dependent tunnel transport.

DOI: 10.1103/PhysRevB.92.224431 PACS number(s): 73.40.Rw, 75.76.+j, 75.70.Kw, 75.78.Cd

I. INTRODUCTION

Magnetic multilayers made of two directly interacting ferromagnetic layers have been at the center of many theoretical and experimental studies [1], by the use of different materials, different magnetic geometries (in plane [2] and out-of-plane [3]), and different experimental technics [4–7]. The main objectives are the development of new functionalities [8,9] and new materials for a wide variety of potential applications: nanoscale composites for hard magnets [10], exchange-coupled composite structures to reduce the switching field amplitude in storage media [11], exchange-coupled multilayers to stabilize hard reference layers in the well-known spin valve structures [12], and future applications in spin-transfer torque-based devices [13]. In the last few years, focus has been made on perpendicular-to-film-plane magnetic configurations since perpendicular recording has effectively replaced traditional in-plane storage media in the hard disk industry [11], and this configuration is more efficient for spin torque phenomena [14].

To date, most of the experimental studies have been based on macroscopic or local magnetization measurements. The impact of the spring magnet configuration in giant magneto resistance [7] or tunnel magneto resistance (TMR) [15] has been scarcely investigated.

In this study, a composite exchange-coupled soft/hard magnetic system ([Co/Pt]/CoTb) exhibiting a wide variety of magnetization reversal processes has been used as the hard electrode in magnetic tunnel junctions (MTJs). The rich and complex behaviors of [Co/Pt]/CoTb as a function of the Pt thickness, temperature, and field history can be reproduced by micromagnetic simulations, based on a detailed investigation of the individual [Co/Pt] multilayers and CoTb layer magnetic properties. The combination of magnetometry and interface-sensitive spin-dependent tunnel transport enables the analysis of [Co/Pt]/MgO/[Co/Pt]/CoTb MTJs' properties and magnetic configurations. Beyond the standard behavior expected in MTJs, this highlights interesting exchange bias, spring magnet and domain duplication phenomena.

II. EXPERIMENTAL DETAILS

The structure of the magnetic tunnel junctions studied in this work is sketched in Fig. 1. The multilayer stackings have been grown on glass substrates in an UHV Alliance Concept sputtering with as base pressure of 5×10^{-9} mbar. After a soft etching of the substrate under pure Ar plasma, a 5 nm-thick Tantalum layer has been first deposited with a deposition rate of 1.2 Å/s, in order to favor the good adhesion of Pt and promote its (111) texture. A 10 nm-thick Pt seed layer is then grown followed by the $[Co/Pt]_3/Co$ stacking (soft electrode), deposited with typical deposition rates of 0.6 Å/s for Pt and 0.09 Å/s for Co. A 2.5 nm-thick MgO insulating barrier (the MgO thickness is the same for all the MTJs discussed in this paper) separates the soft electrode from the hard $[Co/Pt]_3/Co/Co_{86}Tb_{14}$ multilayer. The nominal thickness of the Co layers is the same for all samples, equal to 0.6 nm. The thickness of the Pt layers varies between 1.42 and 2.19 nm. The $Co_{86}Tb_{14}$ layer is 20 nm thick and is referred to as CoTb in the following. Given its high anisotropy, the CoTb is used to pin one electrode by exchange coupling, so that it is possible to get separate reversals for both electrodes. In addition to the MTJ multilayers magnetic properties, the magnetic characteristics of individual $[Co/Pt]_3/Co$ and CoTb layers have been analyzed by magnetometry in order to extract most of their relevant magnetic parameters that will be used for micromagnetic calculations (see Appendix A).

After the growth, a three-step optical lithography process is used to pattern 30 μm × 30 μm junctions and to take electric contacts [Ta(5 nm)/Pt(150 nm)] bilayer on both sides of the MgO tunnel barrier. The electronic transport characteristics have been measured using an "homemade" setup controlled by a Labview interface and composed of an ARS cryostat for the low-temperature measurements (down to 20 K) and an electromagnet that can deliver a magnetic field up to ±2 T.

III. MAGNETIC PROPERTIES IN MTJ FULL STACK

Before the lithography process, the magnetic response of the MTJ full stack has been studied using conventional magnetometry via the measurements of $M(H)$ loops with the magnetic field applied perpendicular to the surface (the easy magnetization axis) and for temperatures between room temperature and 20 K. This is an important step to understand the behavior of the whole multilayer stack, since electronic transport measurements in MTJs are exclusively related to the magnetic response of the electrodes in contact with the tunnel barrier. Magnetization measurements have evidenced some interesting features linked to the $CoTb/[Co/Pt]_3/Co$

*michel.hehn@univ-lorraine.fr

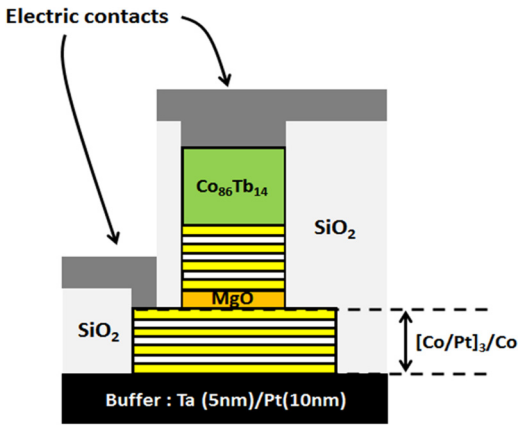

FIG. 1. (Color online) Sketch of the magnetic tunnel junctions.

hard electrode that turn out to be essential in understanding the transport measurements. These are reported below.

A. Magnetization reversal at room temperature

Typical $M(H)$ loops measured at room temperature with the magnetic field applied perpendicular to film plane are presented in Fig. 2 for Pt thicknesses smaller (top left) and larger (bottom left) than 1.73 nm.

These hysteresis loops are typical of measurements along the easy magnetization axis, confirming the strong perpendicular anisotropy in these MTJs (in both $[Co/Pt]_3/Co$ and CoTb layers). Several jumps and steps are observed during the field sweep corresponding to different magnetic configurations for the soft and hard electrodes, reported in Fig. 2 (right). As expected, the reversal of the $[Co/Pt]_3/Co$ multilayer (soft electrode) occurs in a single magnetic switch, whatever the Pt thickness, and is observed at low fields (switch from step A to B). As reported in many studies before, the reversal occurs through nucleation and propagation of reversed domains [16].

The magnetic response of the $CoTb/[Co/Pt]_3/Co$ hard electrode depends on the Pt thickness, as observed in Fig. 2 (left). For Pt thicknesses smaller than 1.73 nm (top left), a single step (from B to D) corresponds to the total magnetization

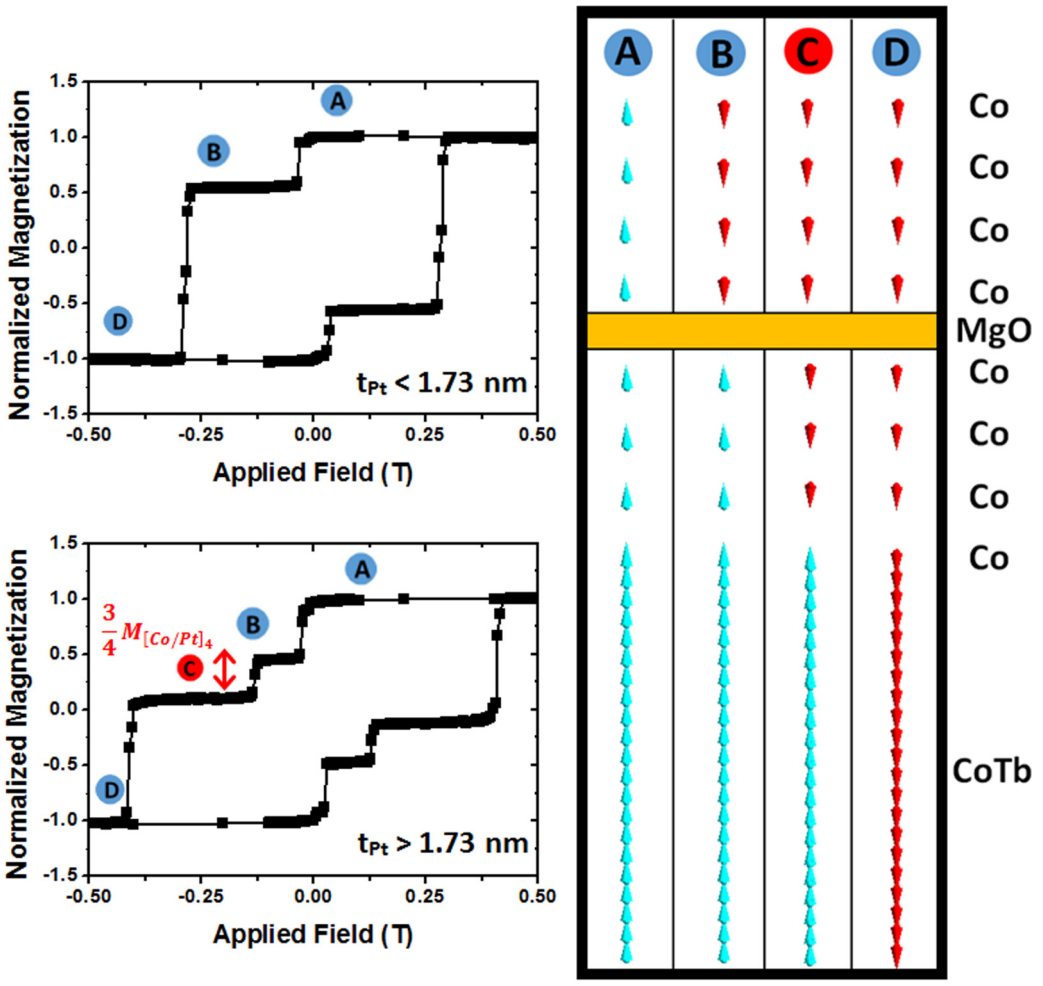

FIG. 2. (Color online) Left: $M(H)$ loops measured at room temperature and with the field perpendicular to the plane for MTJ full stack with Pt thicknesses smaller (top) and larger (bottom) than 1.73 nm. Right: Micromagnetic calculations of the different magnetization configurations for the soft and hard electrodes: A, parallel configuration; B, antiparallel configuration after reversal of the soft electrode; C, intermediary step after partial reversal of the $[Co/Pt]_3$ multilayers in the hard electrode; D, back to parallel configuration.

reversal of the hard electrode. For Pt thicknesses larger than 1.73 nm (bottom left), the hard electrode magnetization reversal occurs in two distinct steps (from B to C and from C to D). A close look at the jump between B and C reveals an amplitude of three-fourths of the $[Co/Pt]_3/Co$ magnetization, showing a partial reversal of the $[Co/Pt]_3/Co$ in the $CoTb/[Co/Pt]_3/Co$ electrode: only three Co layers switch, the last Co layer being pinned to CoTb. Increasing the negative applied field finally drives the simultaneous reversals of the last Co layer in $[Co/Pt]_3/Co$ and of the CoTb layer.

Those two different behaviors can be easily explained, and reproduced using micromagnetic calculations, by the role of the Pt thickness on the coupling between Co layers.

For "thin" Pt layers, the coupling between Co layers is strong and enables the $[Co/Pt]_3/Co$ reversal as a whole. The reversal of the $[Co/Pt]_3/Co$ multilayer is thus complete and leads to the reversal of the CoTb layer.

For "thick" Pt layers, the coupling between the Co layers in the $[Co/Pt]_3/Co$ is weaker. The Zeeman energy leads to the reversal of the three Co layers in the [Co/Pt] multilayers (three-fourths of the $[Co/Pt]_3/Co$ multilayer is reversed), the last Co layer being pinned along the CoTb magnetization and switching with the CoTb at higher applied field. As a result, the $[Co/Pt]_3$ layer is exchange-biased by the Co/CoTb through a Pt layer. The measurement of minor loops for the $[Co/Pt]_3$ reversal enables us to extract the value of the exchange interaction through Pt (results presented in Fig. 10 in Appendix A).

B. Reversal versus temperature and magnetic field history

Beyond the effect of Pt thickness reported above, the temperature is expected to have a significant impact on the magnetization reversal through the temperature dependence of the RKKY coupling and through the hardening of the CoTb layer (see Appendix A). Furthermore, minor loops can lead to complex behaviors where laterally nonhomogeneous magnetic configurations are stabilized. The results presented in this section are obtained for the $[Co_{0.6\,nm}/Pt_{1.42\,nm}]_3/Co_{0.6\,nm}$ based MTJ.

1. Influence of the temperature

The influence of temperature on the M(H) loops for the MTJs full stack has been studied between 300 K and 45 K. At 300 K, the magnetization reversal for the MTJ with 1.42 nm-thick Pt layers occurs in two steps associated to the two electrodes (Fig. 2, top left): as reported previously, the hard electrode reverses as a single block

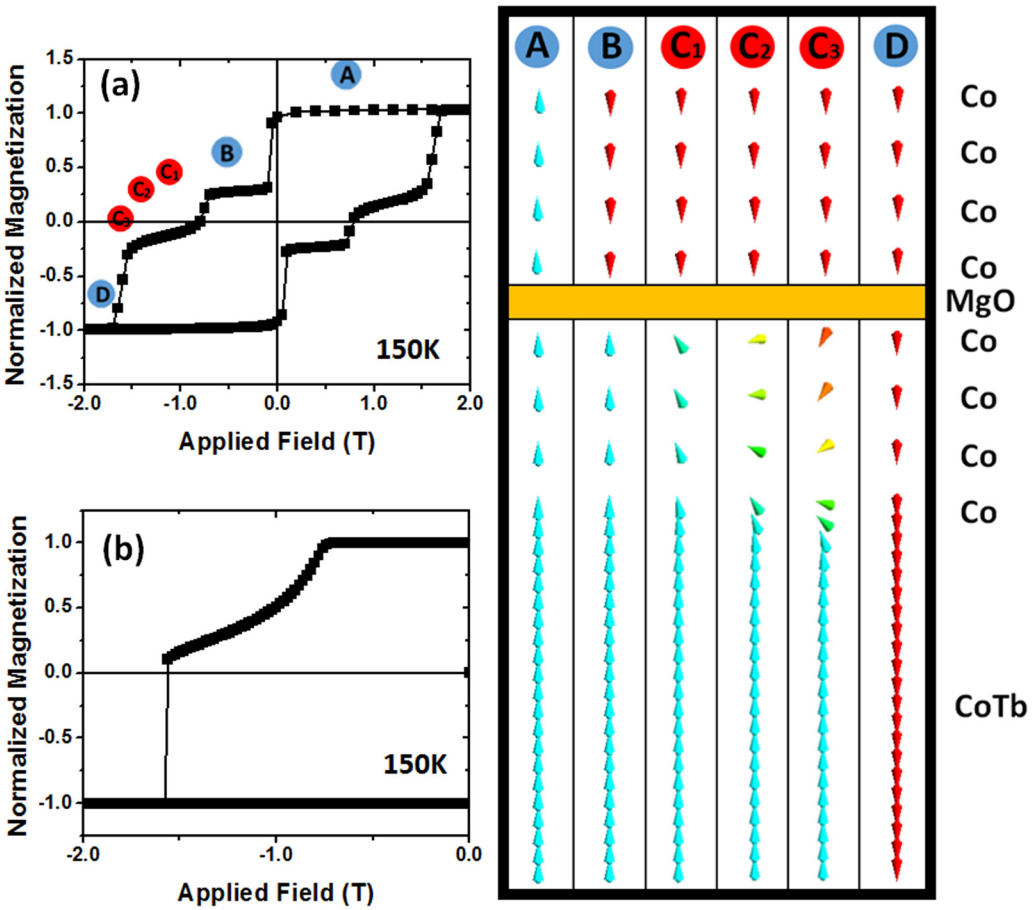

FIG. 3. (Color online) Left: (a) $M(H)$ experimental loop for the MTJ full stack (Pt thickness of 1.42 nm) measured at 150 K. (b) $M(H)$ calculated for the CoTb 20 nm/[Co 0.6 nm/Pt 1.42 nm]$_3$/Co 0.6 nm hard electrode at 150 K. Right: Micromagnetic configurations for the soft and hard electrodes: A, parallel configuration; B, antiparallel configuration after reversal of the soft electrode; C, 1, 2, and 3 reversal of the $[Co/Pt]_3/Co$ multilayer in the hard electrode by the creation of a spring magnet; D, back to a parallel configuration.

since the $[Co_{0.6\,nm}/Pt_{1.42\,nm}]_3/Co_{0.6\,nm}$ multilayer is strongly coupled to $CoTb_{20\,nm}$ by direct exchange. When decreasing the temperature to 150 K and below, the reversal process in the hard electrode changes significantly, with the occurrence of two successive steps [C and D in Fig. 3(a)]. In contrast to the two-step reversal observed in increasing the Pt thickness (Fig. 2, bottom left), the smooth part (labeled C) suggests the development of a spring magnet configuration in the $[Co_{0.6\,nm}/Pt_{1.42\,nm}]_3/Co_{0.6\,nm}$ multilayer in contact with CoTb. This was confirmed by micromagnetic calculations, as shown in Fig. 3 [(b) and right part] using the material magnetic parameter summarized in Appendix A.

This change in the hard electrode magnetic behavior at low temperature is driven by the magnetic properties of the CoTb layer with temperature (Appendix A). When the temperature decreases, the $Co_{86}Tb_{14}$ magnetization decreases and its anisotropy increases [17–19]. In our case, the main consequences are a drastic increase of the effective anisotropy and of the coercive field in the CoTb layer. In this case of small Pt thickness, i.e., large coupling between Co layers, in the $[Co/Pt]_3/Co$ stacking, the high restoring force when the magnetization starts reversing leads to the formation of a spring magnet configuration.

2. *Influence of magnetic field history*

Minor loops have been measured to explore the impact of partial reversal of the hard electrode ($[Co_{0.6\,nm}/Pt_{1.42\,nm}]_3/Co_{0.6\,nm}/CoTb_{20nm}$ electrode). After positive saturation, the field is decreased, reversed to negative values, and stopped at a negative field called H_{rev} in the following, before saturating the system under positive field again. Typical minor loops measured at room temperature and at 65 K are presented in Figs. 4(a) and 4(b), respectively. For the sake of clarity, only a few values of H_{rev} during the hard electrode reversal have been chosen here.

At room temperature [Fig. 4(a)], the value of $H_{rev} = -0.5$ T is sufficient to observe the total reversal of both electrodes, leading to a symmetric $M(H)$ loop, presented in Fig. 2. However, for smaller H_{rev} chosen during the one-step reversal of the hard electrode, an intermediate magnetization state corresponding to a partial reversal can be stabilized. The amplitude of the second jump gives a ratio of approximately 65% and 28% of reversed magnetization for $H_{rev} = -287.5$ mT and $H_{rev} = -282.5$ mT, respectively. This ratio is maintained in the remanent state, i.e., after switching off the applied field.

This specific property for the $CoTb_{20nm}/[Co_{0.6\,nm}/Pt_{1.42\,nm}]_3/Co_{0.6\,nm}$ electrode is likely driven by the reversal mechanism in the CoTb layer. As shown in Ref. [19], switching off the applied field during the reversal process of a 20 nm-thick $Co_{88}Tb_{12}$ layer freezes a magnetic configuration composed of up and down domains. The domain structure persists at the remanence and is therefore responsible for the stabilization of the intermediary magnetization step in the CoTb $M(H)$ loop.

In the MTJ full stack, the $CoTb_{20nm}/[Co_{0.6\,nm}/Pt_{1.42\,nm}]_3/Co_{0.6\,nm}$ hard electrode obviously follows the same behavior, yielding a remanent state with a domain configuration, i.e. with a laterally nonhomogeneous magnetic structure. The soft layer of the MTJ thus reverses in a complex stray field originating from the stabilized domain structure.

At 65 K [Fig. 4(b)], the reversal of the $[Co/Pt]_3/Co$ multilayer of the hard electrode occurs via the development of a spring magnet, as discussed above [Fig. 3(a)]. If the maximum negative applied field H_{rev} is chosen in the range where the spring magnet configuration occurs, i.e., between approx. −1.5 T and −4.5 T, before the reversal of the CoTb part, a perfectly reversible and reproducible behavior is observed in this field range, as expected from the spring magnet behavior.

IV. TRANSPORT PROPERTIES IN PATTERNED MTJS

In the previous section, the magnetic properties of the soft and hard electrodes in the MTJs full stack have been studied by magnetometry. Micromagnetic simulations performed using the magnetic parameters extracted from the individual layers analysis (Appendices A and B) could nicely reproduce experimental observations. The next step consists in exploring the magneto-transport properties in patterned MTJs. The aim is first to investigate how the various magnetic behaviors described above could affect the transport properties and give rise to interesting and original features. The magneto-transport properties are also a fine probe of the magnetic configurations in direct contact with the insulating barrier and thus constitute a powerful tool to complement magnetometry and micromagnetic simulations.

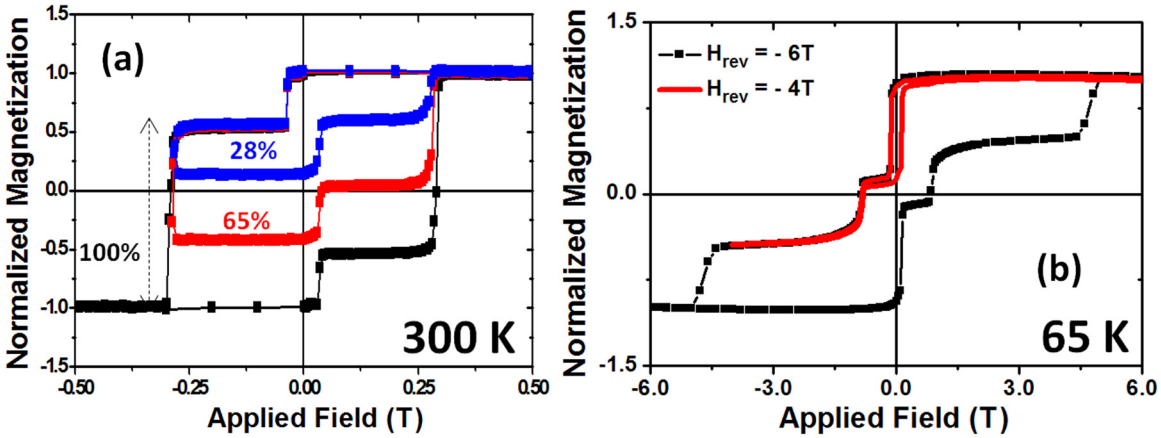

FIG. 4. (Color online) $M(H)$ experimental loops of the MTJ full stack (Pt thickness of 1.42 nm) measured at (a) 300 K for $H_{rev} = -0.5$ T (black squares), −287.5 mT (red squares) and −282.5 mT (blue squares), (b) 65 K for $H_{rev} = -6$ T (black squares) and −4 T (red curve).

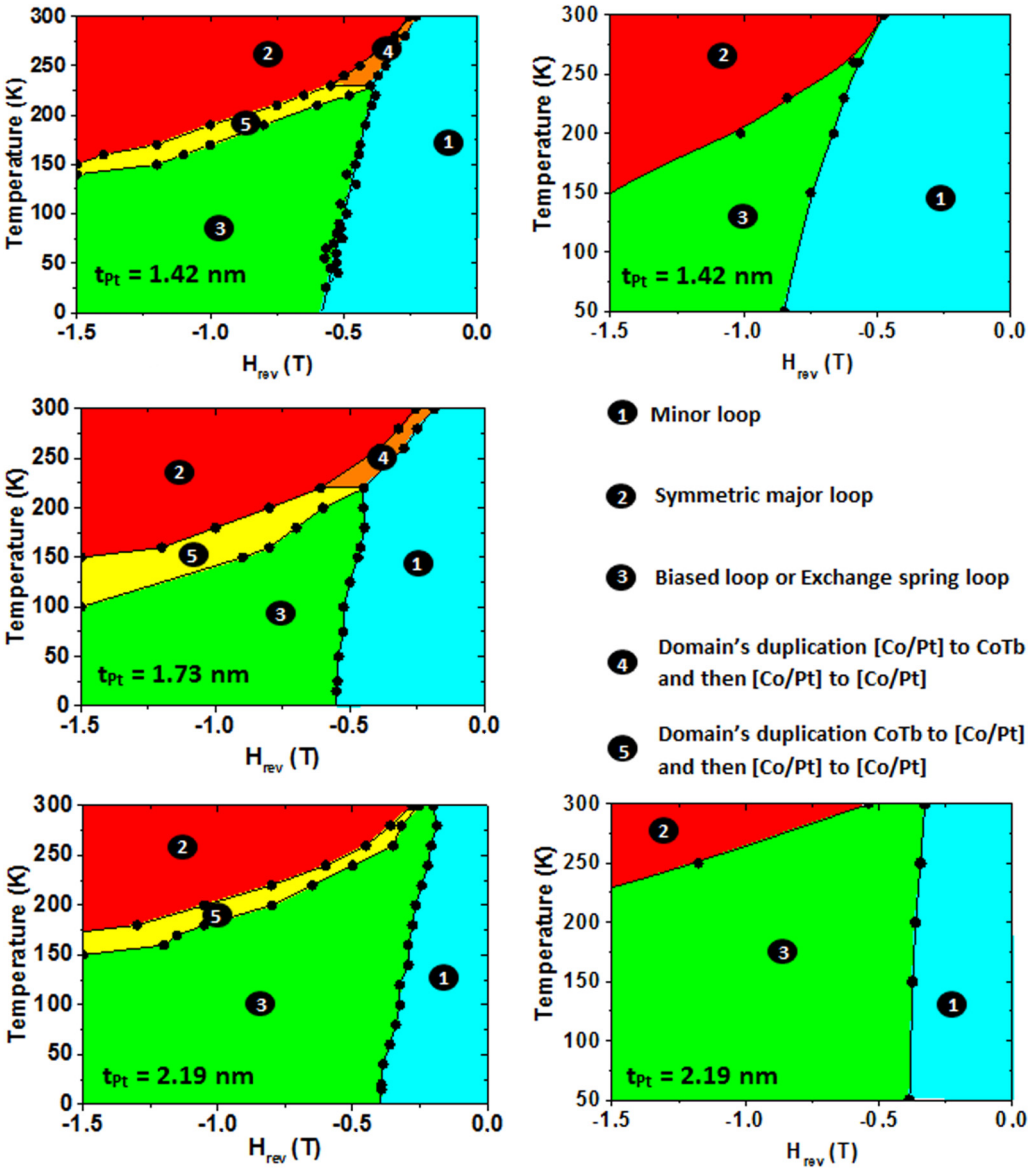

FIG. 5. (Color online) Left: Experimental phase diagrams for the MTJs with Pt thicknesses of 1.42 nm, 1.73 nm, and 2.19 nm. The colored areas referred to different typical behaviors observed by transport measurements $R(H)$ by varying the temperature (T) and the maximum applied negative field (H_{rev}). Right: Calculated phase diagrams for the hard electrodes with Pt thicknesses of 1.42 and 2.19 nm. The colored areas referred to different typical behaviors for $M(H)$ observed by varying the temperature (T) and the maximum applied negative field (H_{rev}).

A. Phase diagrams in patterned MTJs

Since the magnetic state of the hard layer changes with Pt thickness, temperature, and magnetic field history, $R(H)$ transport measurements have been systematically performed on the $[Co_{0.6\,nm}/Pt_{1.42\,nm}]_3/Co_{0.6\,nm}$, $[Co_{0.6nm}/Pt_{1.73nm}]_3/Co_{0.6nm}$ and $[Co_{0.6nm}/Pt_{2.19nm}]_3/Co_{0.6nm}$ based magnetic tunnel junctions, as a function of temperature and H_{rev}.

Starting from saturation under positive field, the influence of the maximum applied negative field value (H_{rev}) on the minor loop has been investigated. Those transport measurements have shown the occurrence of several typical behaviors that can be presented as different colored areas on (T,H_{rev}) diagrams (Fig. 5, left). Those measurements are compared to micromagnetic calculations of the hard electrode magnetization reversal (Fig. 5, right). In the following, the different regions of the diagrams will be discussed.

B. Conventional $R(H)$ characteristics

"Conventional" $R(H)$ characteristics have been measured when H_{rev} is large enough to drive both electrodes reversal (red area on diagrams) and when the value of H_{rev} enables the reversal of the soft electrode only (blue area on diagrams). Those two cases are presented in Fig. 6 for the $[Co_{0.6\,nm}/Pt_{1.42\,nm}]_3/Co_{0.6\,nm}$ based MTJ at room temperature ($H_{rev} = -0.5$ T and $H_{rev} = -0.2$ T). The different magnetic configurations calculated for the soft and hard electrodes are sketched in Fig. 6 (right).

The steps observed in Fig. 6(a) can be correlated to the magnetization steps observed in Fig. 2 (top left) for the MTJ full stack. At high positive field, the low resistance state corresponds to a parallel configuration of both electrodes (sketch A). When decreasing the applied field to negative values, a first jump corresponds to the reversal of the soft

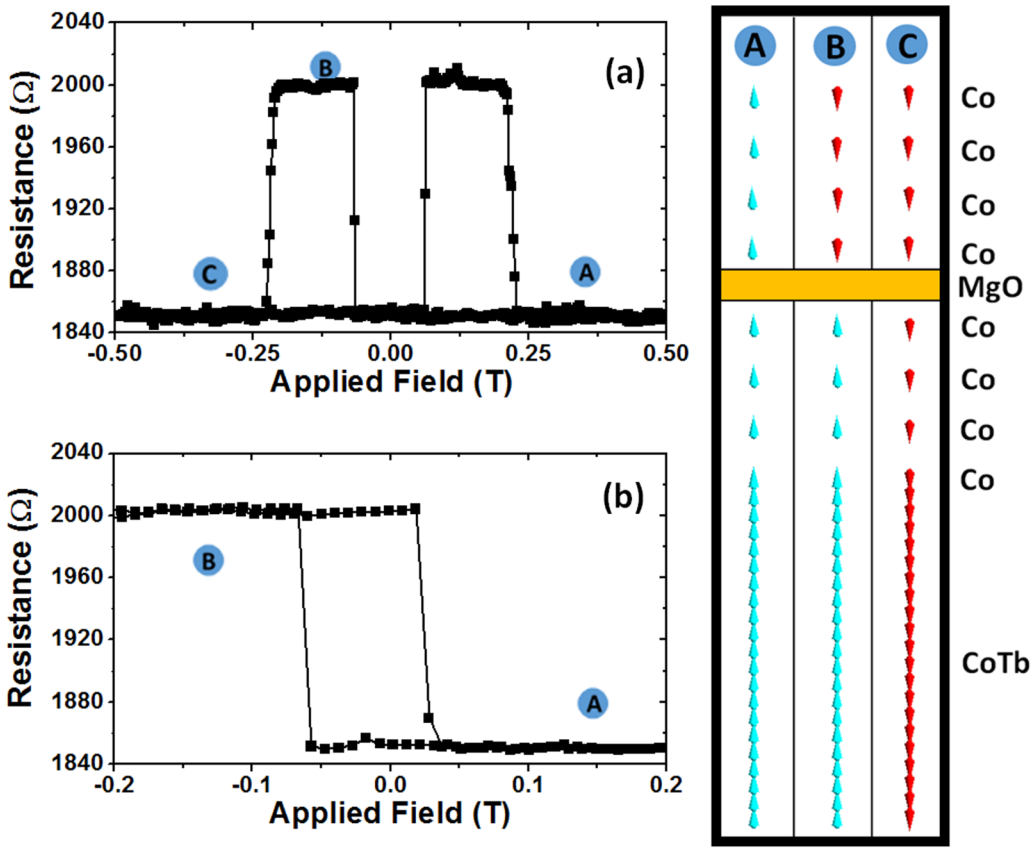

FIG. 6. (Color online) Left: $R(H)$ characteristics for the MTJs with Pt thicknesses of 1.42 nm, measured at room temperature for a reversed field H_{rev} of (a) −0.5 T and (b) −0.2 T. Right: Micromagnetic calculations of the magnetic configurations of the hard and soft electrodes: A, parallel state; B, reversal of the soft electrode (antiparallel state); C, back to a parallel state with the reversal of the hard electrode.

electrode (sketch B). The magnetizations of both electrodes are antiparallel, and thus the resistance becomes high. A further increase of the negative applied field leads to the reversal of the hard electrode and the MTJ goes back to a low-resistance state (sketch C). The symmetric behavior is observed when sweeping the field back from negative to positive values. This behavior corresponds to the "red" areas (large H_{rev} and high temperature) of the phase diagram. If the magnetic field sweep is stopped after the first resistance jump and switched back to positive values, the system stays in a high-resistance state until the positive field is high enough to drive back the magnetization reversal in the soft electrode [Fig. 6(b)]. Only the reversal of the soft electrode is observed. This corresponds to the "blue" areas (small H_{rev}) of the phase diagram for which the magnetic field is not strong enough to reverse neither the $[Co/Pt]_3/Co$, nor the CoTb layer of the hard electrode. In this last case, the soft electrode reversal magnetization loop is slightly shifted along the negative horizontal field axis, as a result of the ferromagnetic coupling between the electrodes across the MgO tunnel barrier. As reported previously in in-plane [20–22] and out-of-plane [23] magnetized MTJs with thick tunnel barriers, this ferromagnetic coupling is attributed to an "orange peel"-type magnetic coupling between both electrodes. This interaction will be particularly important to explain regions of the phase diagram where domain duplication occurs (see Sec. IV D).

The two "classical" behaviors (complete reversal of both electrodes or reversal of the soft electrode only) have been observed at room temperature for all the measured MTJs, whatever the Pt thickness and the reversal mechanism in the hard electrode.

C. Spring magnet and exchange bias behavior

Figure 7 (left) presents the $R(H)$ curves measured in the "green" area ($T = 60$ K) of the diagrams for $[Co_{0.6\,nm}/Pt_{1.42\,nm}]_3/Co_{0.6\,nm}$, $[Co_{0.6nm}/Pt_{1.73nm}]_3/Co_{0.6nm}$, and $[Co_{0.6nm}/Pt_{2.19nm}]_3/Co_{0.6nm}$ based magnetic tunnel junctions.

Those green areas correspond to (T, H_{rev}) ranges where the hard electrode exhibits a two-step reversal (inhomogeneity along the magnetization direction) and where H_{rev} enables the reversal of the $[Co/Pt]_3/Co$ part *only*.

For those H_{rev} values, the CoTb magnetization still points towards the positive field direction but the $[Co/Pt]_3$ magnetization has reversed. The magnetization being thus parallel on both sides of the MgO barrier (sketch A), the system is in a low-resistance state. By increasing the field back towards the positive value, the exchange coupling between the CoTb layer and the $[Co/Pt]_3/Co$ multilayer in contact leads to the first reversal of the $[Co/Pt]_3/Co$ multilayers of the hard electrode (sketch B). The magnetization on both sides of the tunnel barrier being opposite, the resistance state of the system becomes high. The soft electrode finally switches when

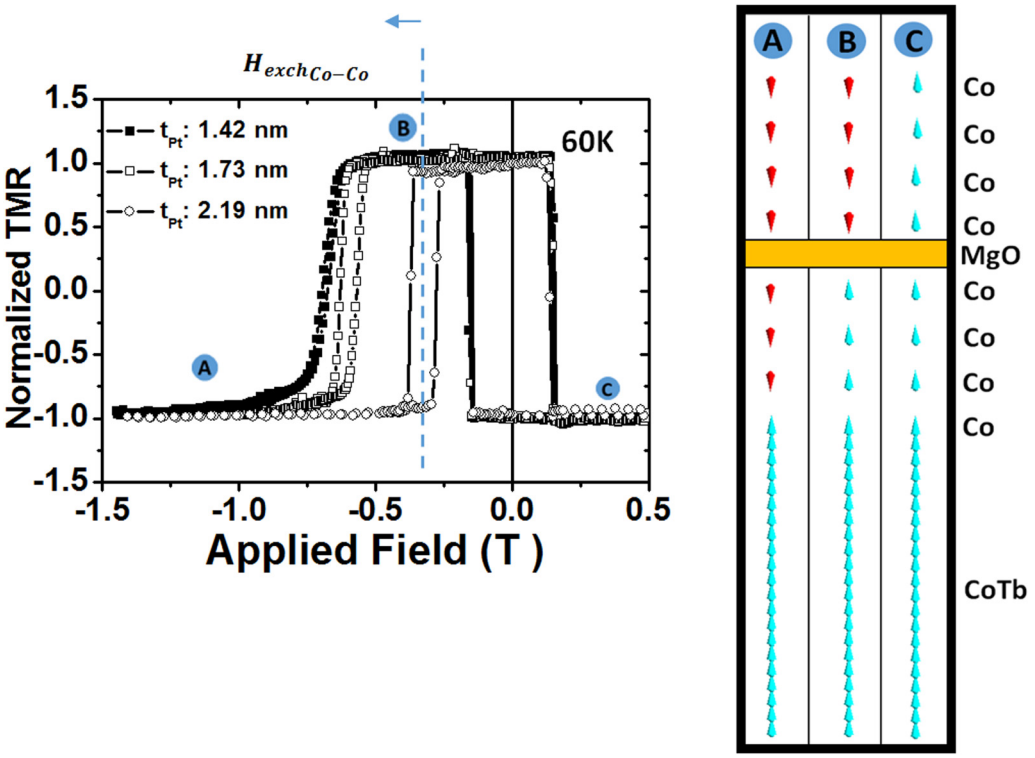

FIG. 7. (Color online) Left: Normalized TMR versus applied field measured at 60 K for MTJs with Pt thicknesses equal to 1.42 nm (filled squares), 1.73 nm (open squares), and 2.19 nm (open circles). Right: Micromagnetic calculations of the magnetic configurations of the hard and soft electrodes: A, reversed soft electrode and partial reversal of the $[Co/Pt]_3/Co$ in the $CoTb/[Co/Pt]_3/Co$ electrode: only three Co layers switch, the last Co layer being pinned to CoTb (parallel state on each side of the tunnel barrier); B, back to homogeneous configuration in the hard electrode (antiparallel state on each side of the tunnel barrier); C, back to a parallel state with the reversal of the soft electrode.

increasing the applied field further (sketch C), and the system goes back to its low-resistance state.

Two limit cases for the $R(H)$ characteristics can be identified in Fig. 7 (left). They correspond to the different two-steps reversal processes identified in the hard electrode by magnetometry measurements and reproduced by micromagnetic simulations.

For "thin" Pt layers (filled squares), the reversible reversal of the $[Co/Pt]_3/Co$ multilayer of the hard electrode as a spring magnet [Figs. 3(a) and 3(b)] leads to a perfectly reversible and reproducible $R(H)$ behavior in the patterned MTJs.

For "thick" Pt layers, the abrupt first reversal of the $[Co/Pt]_3$ multilayer part of the hard electrode (Fig. 2 bottom), the last Co layer remaining pinned to the CoTb, leads to a typical biased loop. The ferromagnetic exchange coupling *through the Pt layer* leads to the horizontal shift of the magnetization reversal observed in Fig. 7 (left). The magnitude of this horizontal shift allows extracting the exchange coupling constant J_{exch} that has been used in the micromagnetic calculations (Fig. 10).

These different results obtained by transport measurements are perfectly in agreement with (1) the magnetic behavior of the hard electrode as a function of Pt thickness and temperature and (2) the predicted phase diagram (Fig. 5, right) obtained by micromagnetic calculations using the magnetic parameters of the $[Co/Pt]_3/Co$ multilayer.

D. Duplication of domains from the hard to the soft electrode

Finally, two supplemental areas ("orange" and "yellow") appear in the MTJs' experimental phase diagrams. They correspond to a specific phenomenon corresponding to the duplication of magnetic domains from the hard electrode to the soft electrode. Such an effect has been previously reported only in the case of in-plane magnetized spin valves and MTJs [20–22]. It arises from the dipolar coupling between the hard and the soft layers through the MgO tunnel barrier as discussed in Sec. IV B. Two different domain duplication processes have been identified, depending on the Pt thickness and temperature. For the sake of clarity, only the symmetric major loop (black) and the loop measured for one value of H_{rev} (red) are reported, at 300 K and 190 K for the $[Co_{0.6\,nm}/Pt_{1.42\,nm}]_3/Co_{0.6\,nm}$ based MTJs (Fig. 8). Those two temperatures correspond to one-step and two-step reversal of the hard electrode, respectively.

Several resistance steps and jumps are observed in Figs. 8(a) and 8(b), and correspond to different magnetic configurations of the soft and hard electrodes. In A, C, and E, the low-resistance state reveals a parallel configuration of both electrodes magnetizations. In B and D, the intermediate resistance states are signature of coexisting parts where the electrodes magnetizations are either in a parallel or antiparallel configuration.

1. Domain's nucleation process in the "orange" area [Fig. 8(a)]

Once the MTJ magnetization is saturated under a magnetic field of +1.5 T, the applied field is decreased to zero and reversed. Increasing the negative applied will lead first to the reversal of the soft [Co/Pt] magnetization.

When H_{rev} enters the field range where the reversal of the hard electrode occurs, magnetic domains form in the

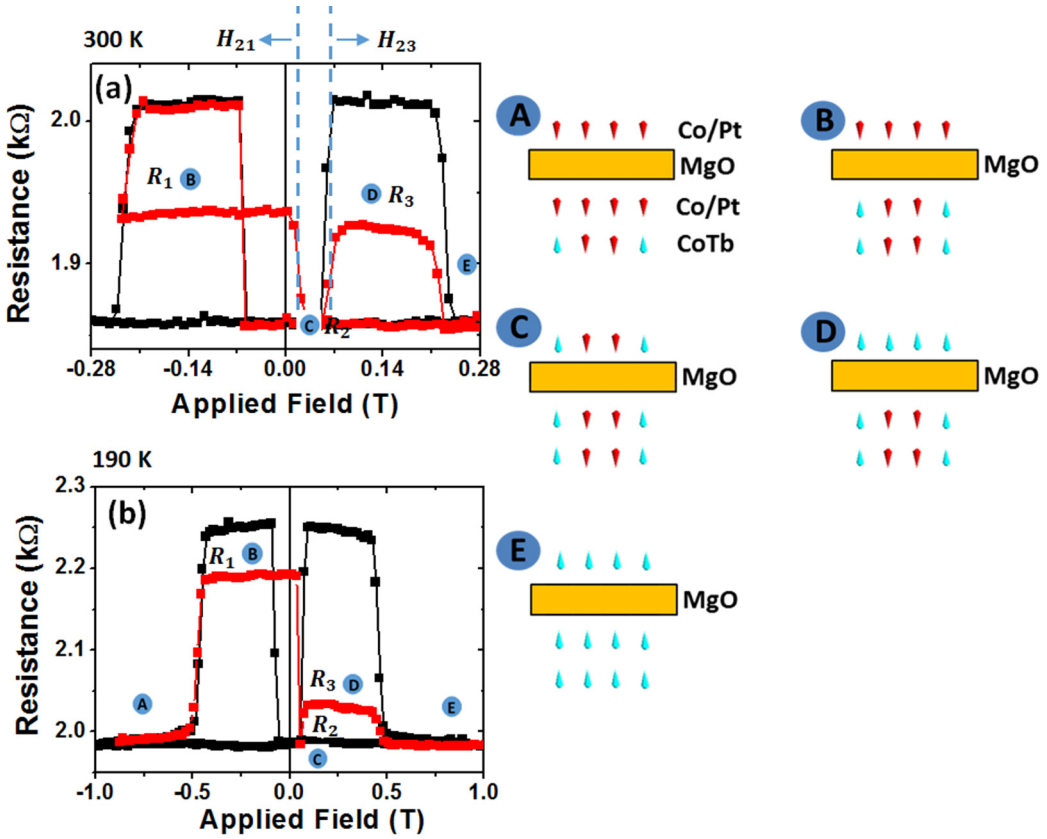

FIG. 8. (Color online) Major loops (black squares) and minor loops (red squares) measured for the MTJ with Pt thicknesses of 1.42 nm at (a) $T = 300$ K ($H_{rev} = -0.3$ T and $H_{rev} = -0.236$ T) and (b) $T = 190$ K ($H_{rev} = -2$ T and $H_{rev} = -0.877$ T). The magnetic configurations for the different resistance steps are sketched in the right part and detailed in the text. The A, C, and E configurations correspond to parallel arrangement across the tunnel barrier, i.e., low resistance states. The B and D configurations correspond to a mixture of parallel and antiparallel arrangements across the tunnel barrier, i.e., intermediate resistance states.

$[Co/Pt]_3/Co$ multilayer in contact with CoTb and propagate into the CoTb layer in a dynamical process (Fig. 8, sketch B). The magnetization in these domains is parallel to the magnetization of the soft electrode, and as a result, increasing the value of H progressively reduces the junction resistance towards the low resistance measured when the magnetizations of both electrodes are parallel. If H_{rev} is chosen during the hard electrode reversal and the applied field is brought back to zero, the junction resistance is kept at an intermediate value R_1, the resistance measured under the applied field H_{rev}. As the single CoTb layer, the CoTb/$[Co/Pt]_3$/Co multilayer obviously keeps the domain structure stabilized at H_{rev}. When the applied magnetic field is reversed to positive values, the magnetic moments of the $[Co/Pt]_3$/Co soft electrode are submitted to a laterally inhomogeneous magnetic field.

The magnetization of the soft electrode under regions where the magnetization of the hard electrode is oriented along the applied field is submitted to an effective field equal to the applied field plus the magnetic stray field of the hard layer: Those regions reverse first for a magnetic field H_{21}. In this state C, the MTJ resistance goes back to the low value R_2 proving that the multidomain structures of both electrodes are perfectly parallel (Fig. 8, sketch C). This phenomenon where the multidomain structure of the hard electrode is "printed" to the soft electrode is called "domains' duplication."

The magnetization of the soft electrode under regions where the magnetization of the hard electrode is oriented antiparallel to the applied field is submitted to an effective field equal to the applied field minus the magnetic stray field of the hard layer: Those regions will reverse in a second step, for a larger applied field H_{23}. The magnetic configuration of the soft electrode turns to be perfectly monodomain again, whereas the domain structure persists in the hard electrode. This results again in coexisting areas where both electrodes magnetizations are either parallel or antiparallel (Fig. 8, sketch D), giving rise to another intermediary resistance state R_3 in the positive field region. Finally, by further increasing the positive applied field, the domain structure in the hard electrode disappears and the MTJ recovers its low, parallel resistance state (Fig. 8, sketch E).

2. *Domain's nucleation process in the "yellow" area [Fig. 8(b)]*

The "yellow" area appears at low temperatures or for large Pt thicknesses and separates the "red" and "green" areas. In the green area, the $[Co/Pt]_3$/Co multilayer in contact with CoTb layer is reversed [exchange-biased $M(H)$ loop for thick Pt layers] or partially reversed (spring magnet behavior for thin Pt layers) while the CoTb layer is not affected by the field (high anisotropy and low magnetization). In these two cases, the parts of the magnetic layers in contact with the tunnel barrier are in a parallel configuration, resulting in a low tunnel

resistance. When increasing H_{rev}, the applied field becomes large enough to drive the partial reversal of the CoTb layer and this corresponds then to the "yellow" area: a domain state starts to nucleate in the CoTb layer (Fig. 8, sketch A). Then, when reducing the field towards zero, the domain state of CoTb duplicates into the $[Co/Pt]_3/Co$ in contact with CoTb, leading to the intermediate resistance value R_1 [Fig. 8(b) and sketch B]. From this state, the same domains duplication process as the one described for the "orange" area occurs from the hard electrode to the soft electrode.

As shown in Fig. 5 (bottom left), this phenomenon is already observed at room temperature for "thick" Pt layers. In this case where the hard electrode magnetization reversal occurs in two separate steps (Fig. 2 bottom left), even at room temperature, it is possible to choose a value of H_{rev} where the $[Co/Pt]_3/Co$ layer has reversed and where the CoTb partial reversal starts with the formation of domains. This domain structure then duplicates into the $[Co/Pt]_3/Co$ in contact and further into the soft electrode. In the case of "thin" Pt layers, the "yellow" area appears for temperatures lower than 225 K, when the magnetization reversals in the CoTb and $[Co/Pt]_3/Co$ layers are no more simultaneous but occur for different magnetic fields, as a consequence of the CoTb increased anisotropy.

V. CONCLUSION

The magnetic properties of MTJs full stack reveal several interesting features, mainly driven by the magnetic properties of the hard electrode. Since the strength of the coupling between the Co layers through the Pt spacer decreases rapidly when the Pt thickness increases, two reversal modes of the hard electrode have been highlighted at room temperature. For thin Pt thicknesses, the simultaneous reversal of the $[Co/Pt]_3/Co$ multilayer and of the CoTb layers is observed whereas for large Pt thicknesses, the reversal occurs in two steps (first reversal of the $[Co/Pt]_3$ multilayer followed by the Co/CoTb reversal for larger applied fields). At low temperatures, the drastic increase of the anisotropy and the decrease of the saturation magnetization in CoTb prevents its reversal, leading either to a spring magnet behavior for thin Pt thicknesses or to an exchange bias behavior for large Pt thicknesses. Finally, by acting on the field history, it is possible to stabilize a remanent intermediate magnetization state with the persistence of domains in the hard electrode. The different magnetic behaviors observed by magnetometry have been reproduced by micromagnetic calculations using the magnetic parameters of the $[Co/Pt]_3/Co$ and CoTb individual multilayers, and summarized in (H_{rev}, T) diagrams. Those can account for the magnetic properties observed in MTJs full stack.

The magneto-transport properties of patterned MTJs have been explored to investigate how the various magnetic behaviors could affect the transport properties and give rise to interesting and original features. Their analysis also constitutes a powerful complementary tool for the study of magnetic configurations, especially at the MgO interface. Beyond the usual cases where the applied field can reverse both electrodes (major symmetric loop) or only the soft one (biased minor loops), the resistance versus magnetic field characteristics have evidenced two interesting behaviors for maximum negative magnetic fields in the range of the hard electrode magnetization reversal: (1) if the magnetic field is large enough to reverse the [Co/Pt] multilayer in the hard electrode but doesn't affect the CoTb layer, the $R(H)$ loops exhibit some common characteristics with $M(H)$, associated to the [Co/Pt] reversal: an exchange biased loop or a reversible spring magnet behavior. This last property is very attractive and could be used in the development of magneto-resistive sensor at room temperature and high fields; (2) if the magnetic field is large enough to reverse the [Co/Pt] multilayer in the hard electrode and part of the CoTb layer, the development of magnetic domains in the hard electrode gives rise to a domains duplication phenomenon from the hard to the soft electrode. This is nicely observed via the occurrence of low-resistance intermediate states.

ACKNOWLEDGMENTS

The authors acknowledge the financial support from FEDER, France, the Region Lorraine, and the Grand Nancy. The authors thank G. Lengaigne for technical support during the nanostructuration of the magnetic tunnel junctions.

APPENDIX A: MAGNETIC PROPERTIES OF INDIVIDUAL LAYERS

A. Co/Pt

The magnetic properties (especially perpendicular anisotropy and saturation magnetization) of the $[Co/Pt]_3/Co$

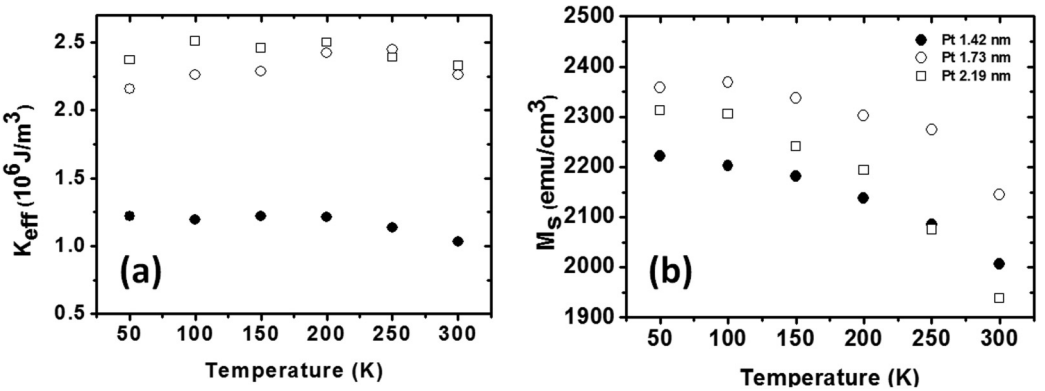

FIG. 9. Temperature dependence of (a) effective anisotropy constant K_{eff} and (b) saturation magnetization per volume unit of Co in $[Co/Pt]_3/Co$ multilayers for different Pt thicknesses.

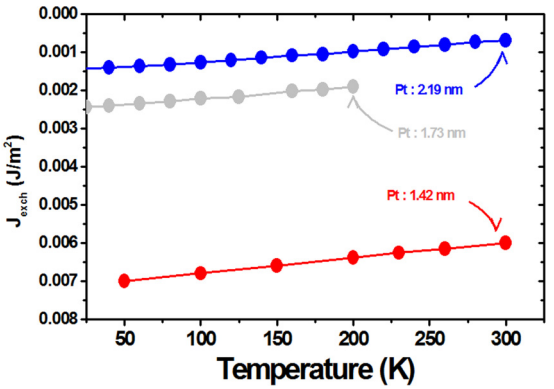

FIG. 10. (Color online) Temperature dependence of the RKKY interaction constant between Co layers through Pt for different Pt thicknesses. The values are deduced (i) from the shift of the $[Co/Pt]_3$ reversal observed in minor loops for $t_{Pt} = 1.73$ nm (gray) and $t_{Pt} = 2.19$ nm (blue), (ii) from the exchange spring response of the CoTb/$[Co/Pt]_3$/Co multilayer for $t_{Pt} = 1.42$ nm (red).

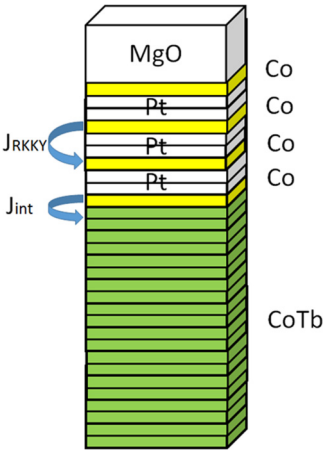

FIG. 12. (Color online) Sketch of the multilayer stack used in the micromagnetic calculations.

multilayer have been investigated separately as a function of Pt thickness and temperature in close connection with structural characteristics [24]. The effective anisotropy constants have been extracted from the M(H) loops via the "area method" [25]. Figures 9(a) and 9(b) present the temperature dependence of the effective anisotropy constant and the saturation magnetization (considering only the volume of Co in the layers) for different Pt thicknesses. For all Pt thicknesses and all temperatures, the effective anisotropy is positive, i.e., perpendicular to film plane magnetization, even if the magnetization strongly increases when the temperature decreases. A complete discussion of those variations is given in Ref. [24]. They are used here mainly as inputs for the micromagnetic calculations. The exchange constant in the Co layers has been chosen equal to 30×10^{-12} J/m, the usual parameter used in OOMMF, and independent of temperature.

Another important parameter is the interaction between the Co layers in the $[Co/Pt]_3$ multilayer, mainly of RKKY origin. This value cannot be extracted from the $M(H)$ loop of the $[Co/Pt]_3$ multilayer. However, when associated to the CoTb layer, the exchange constant (J_{exch}) could be determined for the thickest Pt layers (i.e., 1.73 and 2.19 nm) from the shift of the $[Co/Pt]_3$ reversal observed in minor loops. For the thinnest Pt layers (i.e., 1.42 nm), the coupling constant has been deduced from the exchange spring response of the CoTb/$[Co/Pt]_3$/Co multilayer. Those exchange constants J_{exch} and their variations with temperature for the different Pt thicknesses are given in Fig. 10.

Finally, the temperature-independent exchange constant at the Co/CoTb interface J_{int} has been chosen equal to 15×10^{-12} J/m, an average value between the exchange constants in the CoTb and in the Co layers.

B. CoTb

The magnetic properties of the CoTb alloy have been extensively studied by Gottwald work [17–19]. The exchange constant has been chosen equal to 6×10^{-12} J/m, and independent of temperature. While the saturation magnetization is known, the evaluation of the effective anisotropy is difficult since the magnetic fields to saturate the CoTb films in plane exceed the maximum fields available in our setups. It could be evaluated at room temperature but its variation with temperature has been inferred from the magnetic response of the CoTb/$[Co/Pt]_3$/Co multilayer and from the literature [26].

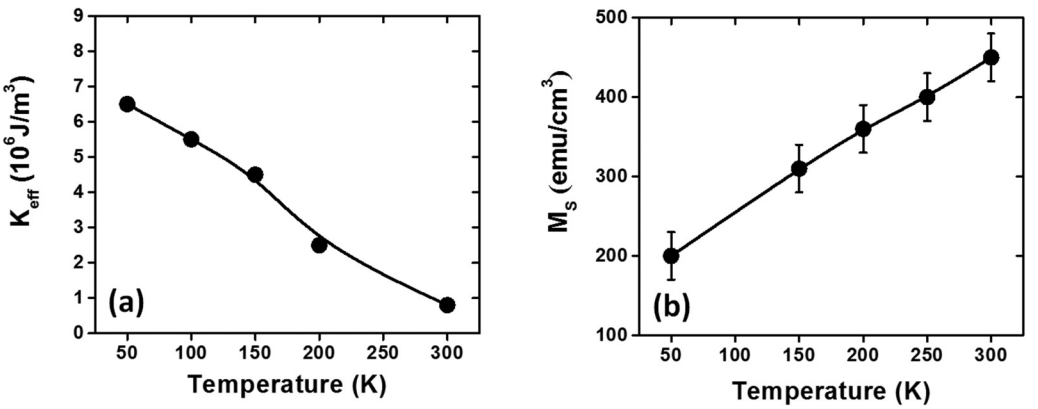

FIG. 11. Magnetic properties measured for the $Co_{86}Tb_{14}$ amorphous alloy. (a) Effective anisotropy constant K_{eff} measured at room temperature and deduced at lower temperature from the magnetic response of the CoTb/$[Co/Pt]_3$/Co bilayer. (b) Saturation magnetization M_s measured as a function of temperature.

The variations of CoTb saturation magnetization and effective anisotropy with temperature are given in Figs. 11(a) and 11(b).

APPENDIX B: MICROMAGNETIC CALCULATIONS

The magnetic response of the hard CoTb/$[Co/Pt]_3$/Co electrode has been simulated using the 3D OOMMF micromagnetic code. In order to reduce calculation time, a pillar of 50 nm × 50 nm has been considered with a cell size of 50 nm × 50 nm × 1 nm. The demagnetization field was not taken into account for these calculations; effective anisotropies that include the demagnetizing field have been used. The multilayer stack used in the micromagnetic calculations is sketched in Fig. 12.

The [Co/Pt] multilayer was treated as 1 nm-thick Co layers (i.e., thickness of one cell) coupled by a RKKY interaction through the Pt layers. The saturation magnetizations and effective anisotropy fields have been extracted from measurements. The CoTb layer was treated as a ferromagnetic layer with saturation magnetization and effective anisotropy fields extracted from measurements.

[1] E. Goto, N. Hayashi, T. Miyashita, and K. Nakagawa, J. Appl. Phys. **36**, 2951 (1965).

[2] E. E. Fullerton, J. S. Jiang, and S. D. Bader, J. Mag. Mag. Mat. **200**, 392 (1999).

[3] S. M. Watson, T. Hauet, J. A. Borchers, S. Mangin, and E. E. Fullerton, Appl. Phys. Lett. **92**, 202507 (2008).

[4] J. McCord, Y. Henry, T. Hauet, F. Montaigne, E. E. Fullerton, and S. Mangin, Phys. Rev. B **78**, 094417 (2008).

[5] S. Mangin, F. Montaigne, C. Bellouard, and H. Fritzsche, App. Phys. A **74**, S631 (2002).

[6] S. Mangin, T. Hauet, P. Fischer, D. H. Kim, J. B. Kortright, K. Chesnel, E. Arenholz, and E. E. Fullerton, Phys. Rev. B **78**, 024424 (2008).

[7] T. Hauet, F. Montaigne, M. Hehn, Y. Henry, and S. Mangin, Appl. Phys. Lett. **93**, 222503 (2008).

[8] R. Skomski and J. M. D. Coey, Phys. Rev. B **48**, 15812 (1993).

[9] R. F. Sabiryanov and S. S. Jaswal, Phys. Rev. B **58**, 12071 (1998).

[10] R. Fischer, T. Leineweber, and H. Kronmüller, Phys. Rev. B **57**, 10723 (1998).

[11] H. J. Richter, J. Phys. D **40**, R149 (2007); N. Supper, D. T. Margulies, A. Moser, A. Berger, H. Do, and E. E. Fullerton, IEEE Trans. Magn. **41**, 3238 (2005); D. Suess, T. Schrefl, S. Fahler, M. Kirschner, G. Hrkac, F. Dorfbauer, and J. Fidler, Appl. Phys. Lett. **87**, 012504 (2005); A. Yu. Dobin and H. J. Richter, *ibid.* **89**, 062512 (2006).

[12] B. Dieny, V. S. Speriosu, B. A. Gurney, S. S. P. Parkin, D. R. Wilhoit, K. P. Roche, S. Metin, D. T. Peterson, and S. Nadimi, J. Mag. Mag. Mat. **93**, 101 (1991).

[13] S. Chung, S. M. Mohseni, V. Fallahi, T. N. Anh Nguyen, N. Benatmane, R. K. Dumas, and J. Åkerman, J. Phys. D **46**, 125004 (2013).

[14] S. Mangin, D. Ravelosona, J. A. Katine, M. J. Carey, B. D. Terris, and E. E. Fullerton, Nat. Mat. **5**, 210 (2006).

[15] Y. Wang, X. Yin, D. Le Roy, J. Jiang, H. X. Wei, S. H. Liou, and X. F. Han, J. Appl. Phys. **113**, 133906 (2013).

[16] J. Ferré, in *Spin Dynamics in Confined Magnetic Structures I, Topics in Applied Physics,* edited by B. Hillebrands and K. Ounadjela (Springer, Berlin, 2002), p. 127.

[17] M. Gottwald, M. Hehn, D. Lacour, T. Hauet, F. Montaigne, S. Mangin, P. Fischer, M.-Y. Im, and A. Berger, Phys. Rev. B **85**, 064403 (2012).

[18] M. Gottwald, M. Hehn, F. Montaigne, D. Lacour, G. Lengaigne, S. Suire, and S. Mangin, J. Appl. Phys. **111**, 083904 (2012).

[19] M. Gottwald, Ph.D. thesis, Nancy University, 2011.

[20] M. Hehn, O. Lenoble, D. Lacour, C. Féry, M. Piécuch, C. Tiusan, and K. Ounadjela, Phys. Rev. B **61**, 11643 (2000).

[21] P. Rottländer, M. Hehn, F. Elhoussine, O. Lenoble, and A. Schuhl, Phys. Rev. B **69**, 064430 (2004).

[22] D. Lacour, M. Hehn, O. Lenoble, A. Schuhl, C. Tiusan, and K. Ounadjela, J. Appl. Phys. **89**, 8006 (2001).

[23] J. Moritz, F. Garcia, J. C. Toussaint, B. Dieny, and J. P. Nozières, Europhys. Lett. **65**, 123 (2004).

[24] M. Bersweiler, K. Dumesnil, D. Lacour, and M. Hehn (unpublished).

[25] M. T. Johnson, P. J. H. Bloemen, F. J. A. den Broeder, and J. J. de Vries, Rep. Prog. Phys. **59**, 1409 (1996).

[26] P. Hansen, C. Clausen, G. Much, M. Rosenkranz, and K. Witter, J. Appl. Phys. **66**, 756 (1989).